Effective Hamiltonian study of $PbZr_{0.95}Ti_{0.05}O_3$

K. Leung,[1] Eric Cockayne,[2] and A. F. Wright[1]
[1]*Sandia National Laboratories, M.S. 1415, Albuquerque, New Mexico 87111-1415*
[2]*Ceramics Division, National Institute of Standards and Technology, Gaithersburg, Maryland 20899-8520*
(Received 23 October 2001; revised manuscript received 25 January 2002; published 17 June 2002)

An effective Hamiltonian H_{eff} is constructed for $PbZr_{0.95}Ti_{0.05}O_3$. It is parametrized using primarily *ab initio* results computed in the virtual-crystal approximation. The phase diagram depends sensitively on the energetic competition between the stable orthorhombic antiferroelectric (A_O) and the metastable ''low temperature'' rhombohedral ferroelectric ($F_{R(\text{LT})}$) structures at 0 K. By incorporating a temperature-dependent thermal-expansion term into H_{eff} and modifying H_{eff} to adjust the relative energies of the A_O and $F_{R(\text{LT})}$ phases, we obtain a ferroelectric phase intervening between the low-temperature antiferroelectric ground state and the high-temperature paraelectric phase, in qualitative agreement with experiments. We also discuss the temperature-dependent disordering of the oxygen octahedral tilts responsible for the experimentally observed space group of the ferroelectric phase.

DOI: 10.1103/PhysRevB.65.214111 PACS number(s): 64.30.+t, 63.70.+h

I. INTRODUCTION

The solid solution $PbZr_{0.95}Ti_{0.05}O_3$ (henceforth PZT 95/5) is antiferroelectric under ambient conditions.[1] This phase has an orthorhombic, 40 atom, unit cell with space group $Pbam$ and is denoted A_O. At 5% Ti, PZT is close in composition to the antiferroelectric-ferroelectric phase boundary at room temperature. (See Fig. 1, adapted from Ref. 1). In PZT 95/5, a rhombohedral ''high-temperature'' ferroelectric phase (''$F_{R(\text{HT})}$,'' with space group $R3m$) exists at ambient pressure and temperature between ≈ 70 and 230 °C, intervening between the low temperature A_O and high-temperature cubic paraelectric (P_C) phases.[1] Both the $F_{R(\text{HT})}$ and P_C phases have five-atom unit cells. Doping with a small amount of Nb is sufficient to make another ferroelectric phase (''low temperature'' ''$F_{R(\text{LT})}$'') the stable phase at ambient conditions.[2,3] Antiferroelectricity is then recovered when hydrostatic pressure is applied.[2,4] Surface charges exist in the ferroelectric phase. Under moderate pressure, as the material becomes antiferroelectric, the surface charges are released as a current.[5] Proximity to the antiferroelectric-ferroelectric phase boundary thus makes PZT 95/5 useful as a pressure-driven power source.

If the Ti content is increased at room temperature, the A_O phase transforms to the $F_{R(\text{LT})}$ phase at about $\sim 6\%$ Ti. This phase has the $R3c$ space group and a ten-atom rhombohedral structure, and exhibits oxygen octahedron rotations about the [111] axis, along which the spontaneous polarization is aligned.[6–19] For Ti compositions near the A_O-$F_{R(\text{LT})}$ phase boundary, the energies of the A_O and $F_{R(\text{LT})}$ structures must be very close and must eventually exhibit a crossover in their ordering. It is reasonable to expect that $F_{R(\text{LT})}$ is metastable for PZT 95/5, and should be relevant to the ferroelectric behavior observed at intermediate temperature. On the other hand, the intermediate ferroelectric phase observed for PZT 95/5 is $F_{R(\text{HT})}$ and not $F_{R(\text{LT})}$. Octahedral oxygen tilts are thus either absent or are thermally disordered.[12–14]

Density functional theory in the local-density approximation (LDA) has proven reliable in predicting the stable structures of perovskite-type ferroelectrics. *Ab initio* calculations assume an added importance for modelling Zr-rich PZT because large single crystals samples of such materials are as yet unavailable. Accurate full-potential linear augmented plane-wave local-density approximation calculations have been used to analyze the stable A_O phase and the $F_{R(\text{HT})}$ structure in lead zirconate (PZ).[20] Supercell studies of ordered PZT structures have been successfully performed, although they are typically done for the 50/50 composition.[18,21,22] Studies of phonon dispersions for pure

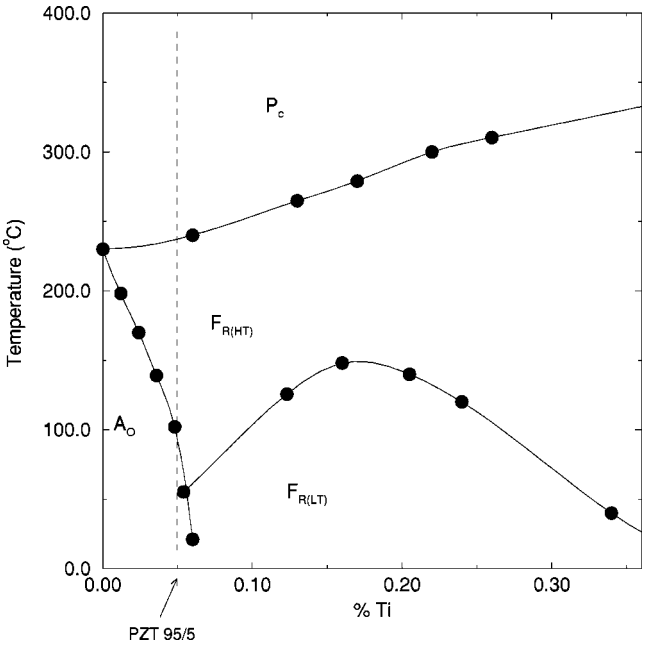

FIG. 1. Temperature-composition phase diagram of high Zr content PZT. A_O: antiferroelectric orthorhombic phase with $Pbam$ space group and 40-atom unit cell; $F_{R(\text{LT})}$: low-temperature rhombohedral ferroelectric phase, $R3c$ space group and ten-atom unit cell; $F_{R(\text{HT})}$: high-temperature rhombohedral ferroelectric phase, $R3m$ space group, five-atom unit cell; P_C: cubic paraelectric phase, five-atom unit cell. The circles are experimental phase boundary points taken from Ref. 1; the lines are a guide to the eye.

PZ (Ref. 23) have shed significant insight into the temperature-composition phase diagram of Zr-rich PZT. The phonon dispersion for PZ in the high-temperature cubic phase contains instabilities across the entire Brillouin zone.[23,24] The various low-temperature phases in the PZT phase diagram are obtained by freezing in one or more of these unstable modes. Competition and cooperation between these instabilities, which depends on their anharmonicities and couplings, determine the relative phase stabilities at a particular composition.

Temperature-dependent properties such as phase stabilities, spontaneous polarization, and piezoelectric properties are too costly to compute directly from first principles (e.g., via *ab initio* molecular dynamics). To study finite-temperature effects and at the same time retain the reliability of first-principles predictions, the *ab initio* effective Hamiltonian approach has been used extensively.[25–29] This approach replaces the classical lattice Hamiltonian with an effective Hamiltonian, generally based on a reduced set of degrees of freedom. The effective Hamiltonian has the form of a Taylor expansion about the cubic perovskite phase, and the parameters are determined by fitting to appropriate regions of the *ab initio* potential-energy surfaces. *Ab initio* effective Hamiltonians have been applied to study PZ,[29] which is fairly similar to PZT 95/5. The effective Hamiltonian constructed in that work leads to distortions from cubic symmetry in qualitative agreement with experiments, but its low-temperature behavior is not completely resolved.

In this work, we parametrize an effective Hamiltonian H_{eff} for PZT 95/5, paying particular attention to the stable and metastable structures and energetics which can be directly fitted to LDA calculations. We use the virtual-crystal approximation (VCA), where the pseudopotentials for the *B*-site Zr/Ti atoms in PZT 95/5 are replaced by a weighted average of both.[30] In this approximation, PZT 95/5 and PZ have very similar zero-temperature structures. The stable structures of both PZ and PZT 95/5 have similar 40-atom orthorhombic cells. The atoms are displaced from their ideal perovskite positions by a superposition, predominantly, of one of the six equivalent Σ_3 modes and an R_{25} phonon mode with [110]-type polarization.[31] The relaxed LDA atomic positions for PZ are in good agreement with experiments.[20,32–34] As mentioned above, other phonon modes are also unstable,[23] including the Γ_{15} modes which would give ferroelectric behavior. However, only R_{25} and Σ_3 (plus trace amplitudes of R_{15}-, P_3-, X_1-, and $M_{5'}$-like distortions) appear at zero temperature and ambient pressure. (A recent *ab initio* simulation shows that substantial M_3-like distortions exist at high pressure.[32])

Given the similarity between PZ and PZT 95/5 at low temperature, the advances made in a previous effective Hamiltonian study of PZ are applied whenever possible.[29] As before, to harmonic order, the interatomic interactions are given by the interatomic force matrix (IFM), while anharmonic terms are fitted to *ab initio* supercell results using polynomials. To increase accuracy, we also depart slightly from many existing effective Hamiltonian works, as follows: (a) the lattice Wannier function approach[35] is not used; (b) the number of degrees of freedom in the harmonic part of H_{eff} is not reduced (i.e., 15 degrees of freedom are retained per primitive cell containing five atoms); and most significantly (c) the energy difference between the A_O and $F_{R(\text{LT})}$ structures is adjusted by a few meV per formula unit away from the *ab initio* value, instead of leaving it as a prediction as was done in Ref. 29. This last point is critical because, as will be shown, the antiferroelectric-ferroelectric phase transition depends sensitively on the relative energies between the stable A_O and the metastable $F_{R(\text{LT})}$ phases. Our philosophy reflects a compromise between the usual *ab initio* effective Hamiltonian approach and the traditional atomistic approach which fits two- and three-body potentials, the functional forms of which are motivated by asymptotic physical considerations. The former approach recognizes that the zero-temperature stable structure, and the phase space visited by the system at low temperature, are close to the cubic, ideal perovskite atomic configuration, and hence small Taylor expansions should suffice. This affords great accuracy and flexibility to formulate the effective Hamiltonian. However, Taylor expansion may not very accurately reproduce the relative energetics of phases which have significantly different atomic configurations. These energies are typically used to parametrize atomistic potentials. As will be shown, explicitly including them in constructing the effective Hamiltonian is pertinent and advantageous.

Our goal is to obtain a model that captures the PZT 95/5 stable phase and its phase diagram. Effective Hamiltonians generally predict phase transition temperatures which can be off by as much as hundreds of kelvin.[25,28] Since the $F_{R(\text{HT})}$ phase spans less than 200 K for PZT 95/5, this becomes a serious concern, because a qualitatively incorrect phase diagram may be obtained. To avoid this, we have fitted away from LDA results in several instances to improve agreement with experiments. We also highlight the issue of thermal expansion which is difficult to incorporate into effective Hamiltonians. This is crucial for the existence of a ferroelectric phase within the context of our H_{eff}. Notwithstanding these changes, given the large and diverse set of parameters required merely to arrive at the zero-temperature phase, it would have been impossible to obtain a model sufficiently close to experimental results if we did not adhere closely to *ab initio* results.

This paper is organized as follows. Section II describes some first-principles predictions for the A_O, $F_{R(\text{LT})}$, and $F_{R(\text{HT})}$ structures. The construction of H_{eff} is discussed in Sec. III. Section IV compares the predicted zero-temperature properties with *ab initio* VCA predictions. The finite-temperature properties are described in Sec. V, and Sec. VI concludes the paper with further discussions.

II. FIRST-PRINCIPLES CALCULATIONS

Density-functional theory in the local-density approximation is used throughout this work. We use a plane-wave, pseudopotential, method within the virtual crystal approximation to compute the ground state properties of PZT 95/5. Hamann,[36] Troullier,[37] and optimized pseudopotentials[38] are used for Pb, O, and Zr/Ti atoms, respectively. A nonlinear partial core correction[39] with a core radius of 2.1 a.u. is

TABLE I. PZT 95/5 cubic and rhombohedral phases lattice constants, atomic displacements, and energies. Displacements are in units of the lattice constant along one of the cubic lattice directions, and are referenced to Pb ion positions. Zr/Ti displaces along the [111] direction, while (for $F_{R(\mathrm{LT})}$) O rotates around the [111] direction in addition to moving closer to Pb. For the $F_{R(\mathrm{LT})}$ phase, calculations are performed on fcc supercells containing two formula units, using $4\times4\times4$ Monkhorst-Pack Brillouin-zone sampling. "O_2" in successive crystal planes exhibits alternating displacements in this structure, consistent with condensation of R_{25} modes.

	$\delta_{\mathrm{Zr/Ti}}$	δ_{O1}	δ_{O2}	δE	a (Å)	$\Delta\alpha$
cubic	0.0000	0.0000	0.0000	0.000 eV	4.1137	0.0000°
$F_{R(\mathrm{HT})}$	0.0553	−0.0714	−0.1015	−0.3300 eV	4.1435	0.2669°
$F_{R(\mathrm{LT})}$	0.0769	−0.0530	−0.0797±0.0580	−0.3909 eV	4.1117	0.067°

included for Pb, while inner-shell pseudovalent electrons (i.e., $4s$ and $4p$ for Zr and $3s$ and $3p$ for Ti) are explicitly treated for the *B*-site atoms. The details of the well-tested Zr and Ti pseudopotentials are described in the literature.[26,29] Monkhorst-Pack[40] grids similar to $6\times6\times6$ Brillouin sampling for a five-atom primitive cell are used in the strain-relaxed ground state calculations (e.g., a $4\times2\times3$ grid for the 40-atom A_O structure), while supercell calculations performed to investigate phonon anharmonicities use Monkhorst-Pack grids similar to primitive-cell $4\times4\times4$ grids.

The VCA equilibrium lattice constants are listed in Table I. The cubic phase lattice constant is 0.18% larger than a Vegard law interpolation between corresponding $PbTiO_3$ and $PbZrO_3$ results. Table I also lists the VCA relaxed structure of the two rhombohedral ferroelectric structures. The $F_{R(\mathrm{HT})}$ atomic displacements for PZT 95/5 are within 10% of the *ab initio* results for PZ.

$F_{R(\mathrm{LT})}$ is obtained from $F_{R(\mathrm{HT})}$ by condensation of oxygen octahedral rotation around the [111] axis. Such a superposition of ferroelectric Γ_{15}-like displacements and R_{25}-like oxygen rotations yields a C_{3v} symmetry about the [111] direction, a doubled (ten-atom) unit cell, and a further energy reduction of 61 meV compared to the five-atom unit cell $F_{R(\mathrm{HT})}$ structure. The magnitude of the predicted Zr displacement relative to Pb in the $F_{R(\mathrm{LT})}$ structure is considerably higher than that found experimentally for PZT 90/10,[7,10] where $F_{R(\mathrm{LT})}$ is the stable phase. This is consistent with the fact that this displacement increases with decreasing Ti content.[10] At zero temperature $\Delta\alpha$, the deviation of the rhombohedral cell angle α from the ideal cubic 90° is 0.066°, which is a factor of 4 smaller in $F_{R(\mathrm{LT})}$ than in $F_{R(\mathrm{HT})}$.

The $F_{R(\mathrm{HT})}$ structure is much higher in energy than the $F_{R(\mathrm{LT})}$ structure for PZT 95/5. Similar conclusions have been drawn for PZ (Ref. 32) and PZT 60/40.[21] Furthermore, Fig. 2 shows that $F_{R(\mathrm{HT})}$ is *unstable*, not metastable, with respect to R_{25} distortions.[41] The instability persists under significant tensile strain. We conclude that $F_{R(\mathrm{HT})}$ *does not* play a pivotal role in the antiferroelectric-ferroelectric phase transition we are interested in. Instead, the competition between $F_{R(\mathrm{LT})}$ and A_O should largely govern that phase transition. On the other hand, neutron and x-ray scattering experiments on PZT 95/5 reveal that the ferroelectric phase is $F_{R(\mathrm{HT})}$. The apparent paradox between first-principles energetics and experimental observations are reconciled if, at room temperature, the R_{25} octahedral tilts are spatially disordered and average to zero within microscopic length scales. The predicted atomic positions of the A_O phase are tabulated in Table II. The 40-atom orthorhombic cell exhibits period doubling of Pb atom positions, which is observed in recent neutron scattering experiments on PZ.[34] The energies of the A_O and $F_{R(\mathrm{LT})}$ phases are extremely close, as expected from the experimental observation that increasing the Ti-content slightly from the 95/5 composition makes $F_{R(\mathrm{LT})}$ more stable than A_O. Our *ab initio* calculations predict that the energies of the A_O and $F_{R(\mathrm{LT})}$ structures are within 3.3 meV per formula units of each other. Given the uncertainty inherent in the

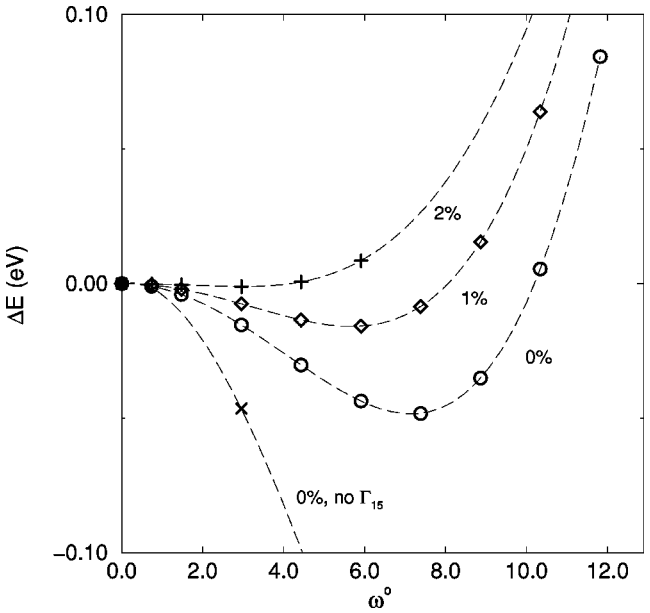

FIG. 2. Energy per formula unit as function of the octahedral oxygen tilt about the [111] direction (ω), or equivalently, the R_{25} amplitude, predicted using the LDA. The lattice constants are fixed at the equilibrium cubic lattice constant (a_o), $1.01a_o$, and $1.02a_o$; cubic cells are used throughout. At each cell volume, the atomic positions are first fully relaxed for a [111]-polarized Γ_{15} distortion while constraining $\omega=0$. This yields a $R3m$ crystal space group. Then ω is incrementally increased yielding a $R3c$ space group, and the energy obtained is referenced to the structure with $\omega=0$. Also shown are results without ferroelectric distortions, i.e., where R_{25} oxygen tilts are the only atomic displacements allowed.

TABLE II. PZT 95/5 orthorhombic phase atom positions, with the LDA, in the virtual-crystal approximation. The experimental lattice constants at room temperature are 5.884, 11.768, and 8.220 Å, respectively (Ref. 50).

a, b, c	5.8190	11.7156	8.0919
$Pb1_{x,y,z}$	0.6976	0.1226	0.0000
$Pb2_{x,y,z}$	0.7100	0.1271	0.5000
$Zr_{x,y,z}$	0.2422	0.1248	0.2498
$O1_{x,y,z}$	0.2809	0.1603	0.0000
$O1'_{x,y,z}$	0.3080	0.0915	0.0000
$O2_{x,y,z}$	0.0385	0.2836	0.0000
$O3_{x,y,z}$	0.0000	0.5000	0.1976
$O4_{x,y,z}$	0.0000	0.0000	0.2285

VCA, pseudopotentials, and the LDA itself, the relative energies of two completely different structures cannot be determined to such accuracy. It is more profitably treated as a fitting parameter which can be adjusted to tune the antiferroelectric-ferroelectric transition temperature of H_{eff}—an option which will be pursued in this work. Nonetheless, VCA-LDA does correctly predict A_O to be the more stable structure in PZT 95/5.[42]

III. CONSTRUCTION OF H_{eff}

We start with PZT 95/5 in the cubic perovskite structure, perform Taylor expansions, and map out the LDA potential energy landscape with respect to harmonic and anharmonic atomic displacements and strain. Strain-phonon couplings are also included in ways similar to previous effective Hamiltonian works.[25,26] In several instances we also fit away from LDA results.

A. Harmonic interactions

The cubic phase interatomic force constants are computed for a $4\times4\times4$ wave-vector grid using density-functional perturbation theory.[43] The long-range dipolar interactions are incorporated in the usual way, via Born effective charges $Z^\star$ and the electronic dielectric constant ϵ_∞.[44] $Z^\star$ and ϵ_∞ for PZT 95/5 are similar to published results for PZ.[29] In PZT 95/5, as in PZ, there are unstable phonon modes across the entire Brillouin zone. In this paper, we will focus on the eigenvalues of the interatomic force matrix computed at the equilibrium VCA lattice constant of the unstable cubic phase, rather than the phonon frequencies themselves. The latter provides a direct comparison with experiments. In the absence of quantum effects, however, the masses that go into phonon calculations are irrelevant to phase diagrams and equilibrium behavior, and one might expect IFM eigenvalues to give a more consistent ranking of instabilities. There are minor differences between the phonon and IFM eigenvalue dispersions. For example, the $M_{5'}$ modes have a more negative IFM eigenvalue than the M_3 modes, while the reverse is true of the respective phonon modes. One might expect that regions in the Brillouin zone with the most negative IFM eigenvalues should determine the distortions that occur at zero temperature. Figure 3(a) shows otherwise. The most negative eigenvalues occur in the Γ_{15} and $M_{5'}$ modes. No lattice displacements with such superlattice modulations are observed in the stable A_O phase. Instead, lattice displacements with Σ_3 (1/4,1/4,0) and R_{25} symmetries are observed, and neither of these wave vectors appear to be local minima in the plot. To understand the observed distortions in the stable A_O phase, anharmonicities must also be examined.

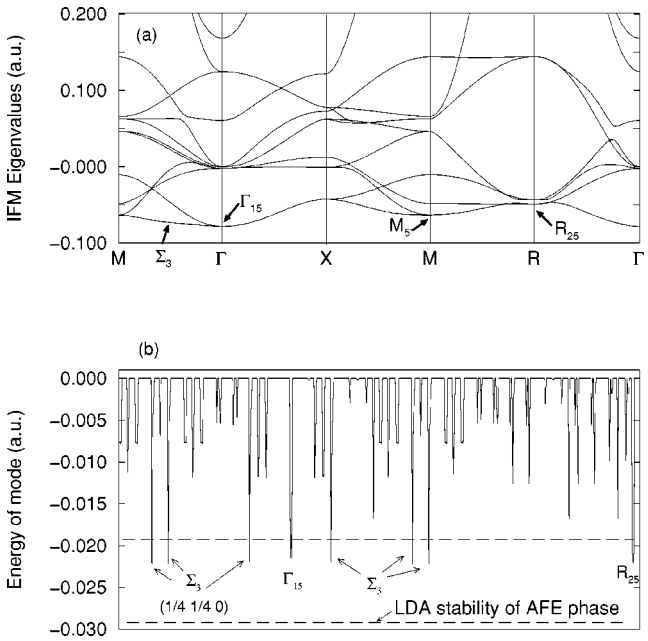

FIG. 3. (a) Eigenvalues of the interatomic force matrix, in atomic units, across the Brillouin zone. The LO-TO splitting is already incorporated at this level, as is evident from the doubly degenerate transverse optical Γ_{15} modes; in the absence of this splitting, these modes are triply degenerate. (b) Minimum energy for each Fourier mode computed from effective Hamiltonian by constraining the amplitudes of all but that mode to be zero. The modes span a $4\times4\times4$ supercell and are grouped by their wave vector. 576 of the possible 960 modes are depicted; the six highest-energy modes at each point in the Brillouin zone have been omitted because they are always stable. Zero energy indicates a stable mode.

B. Anharmonic interactions

As in standard effective Hamiltonian approaches,[25–27,29] the anharmonicities are modeled as polynomials that contain even powers of the lattice distortions. To simplify the treatment of anharmonic terms, we make a change of coordinates by projecting the atomic displacement coordinates onto a basis set consisting of various localized atomic displacement patterns. The localized displacement patterns take the place of the lattice Wannier functions in Ref. 29 and the amplitudes of the basis functions become the arguments of the potential-energy polynomials.

There is considerable freedom in choosing the localized basis set. The pertinent criteria are as follows. (a) Reproducing high symmetry lattice displacive eigenmodes and energies. In this work, we tailor individual local displacement patterns to each of the Γ_{15}, Γ_{25}, X_3, M_3, M_5', and R_{25}

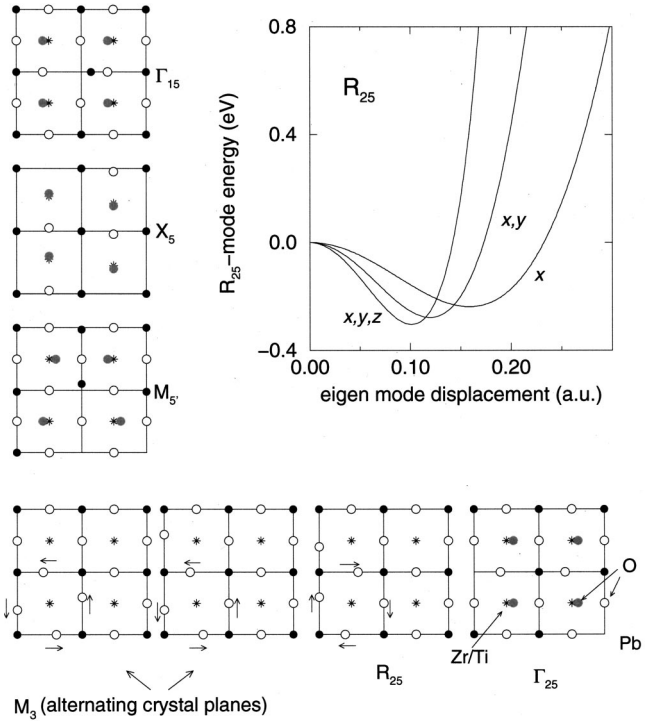

FIG. 4. Localized basis sets used in computing the anharmonic contributions involving Γ_{15}-, Γ_{25}-, X_5-, M_5'-, M_3-, and R_{25}-like displacements. The M_5' basis function has longer-ranged contributions than is shown here. The R_{25} local variable governs both M_3 and R_{25} anharmonicities; the M_3 basis function itself is only used for cross-coupling terms. Also shown is the potential energy surface for the freezing in R_{25} modes in the [100], [110], and [111] directions. Energies and displacements are in atomic units.

modes (Fig. 4). (b) Maximum localization. (c) Orthogonality, to the extent possible. This last feature mimics lattice Wannier functions, which are strictly orthogonal. [As a compromise between (b) and (c), the local displacement patterns associated with R_{25} and M_3 are not orthogonal.] By satisfying the above criteria, the anharmonic coefficients are easily computed by fitting a series of supercell energies for various distortion amplitudes involving one or more high-symmetry modes.[26,29] The specific functional forms and parameters of $H_{\text{anharmonic}}$ are described in the Appendix. Anharmonicities associated with non-zone-boundary, non-zone-center displacements are not explicitly treated. Within our effective Hamiltonian framework, their anharmonic behavior is essentially obtained via interpolation.

For Zr-rich PZT, it is crucial to include cross-couplings between unstable displacive modes at *different* points of the Brillouin zone.[29] These are fitted using polynomials at least second order in both types of local distortions. Consider one-site toy Hamiltonians of the form

$$H = H_A + H_B + H_{\text{int}}, \tag{1}$$

$$H_A = \sum_{i=x,y,z} a_2 A_i^2 + a_4 A_i^4,$$

$$H_B = \sum_{i=x,y,z} b_2 B_i^2 + b_4 B_i^4,$$

$$H_{\text{int}} = \sum_{i,j=x,y,z} c_{2ij} A_i^2 B_j^2,$$

where A and B denote local distortion amplitudes associated with modes A and B. To determine all coupling components c_{2ij} would require large supercells and numerous calculations. To the extent that the details of c_{2ij} are not important to the phase transformation behavior of H_{eff}, we replace each c_{2ij} tensor by a single ''isotropic'' coupling parameter c_2. Similar simplifications are used for the other intermode coupling terms.

To calculate c_2, we freeze in all Cartesian polarization components of one of the modes. The amplitude of this mode (say A) is held fixed, at its optimal value. The amplitude of the other mode (B) is then increased from zero and the results are fit to a polynomial. We generally freeze one Cartesian component of the polarization for this second mode, except for the R_{25}-Γ_{15} coupling, where all three components of both modes are simultaneously frozen in. This procedure generally yields repulsive biquadratic cross-terms. Finally, to obtain the correct relative metastable phase energies, we slightly alter the biquadratic cross-term parameters. Thus the Γ_{15}-R_{25} cross-term fixes the $F_{R(\text{LT})}$ energy, while Γ_{15}-X_3, R_{25}-M_3, and R_{25}-$M_{5'}$ terms are proportionately increased to yield a reasonable A_O energy.

An ''isotropic'' description of Γ_{15}-R_{25} coupling is not adequate for PZT 95/5 because it does not properly align the polarizations of Γ_{15} and R_{25} in the $F_{R(\text{LT})}$ metastable phase. To obtain the correct $F_{R(\text{LT})}$ structure, we project local Γ_{15} and R_{25} distortions onto all four of the body-diagonal axes, namely, [111], [$1\bar{1}\bar{1}$], [$1\bar{1}1$], and [$\bar{1}11$]. The projections Γ_i^P and R_i^P, $i=1,\ 2,\ 3$, and 4, are coupled biquadratically,

$$E_{\Gamma-R}^{(\text{aniso})} = c^{(\text{aniso})} \sum_{ij=1,4} (1 - 5\delta_{ij}/2) \Gamma_i^P R_j^P, \tag{2}$$

with the coefficient $c^{(\text{aniso})}$ given in the Appendix. This is the only instance in our H_{eff} where anisotropy is invoked in the anharmonic cross-terms.

As mentioned above, the most unstable modes of the IFM do not include the distortions experimentally observed in stable A_O phase. It is instructive to perform a mode-by-mode analysis in the presence of the anharmonic terms. We use a $4\times4\times4$ supercell, take the eigen modes of the interatomic force constants as degrees of freedom, and proceed to minimize the energy with respect to the amplitudes of these modes one at a time, keeping all others zero. The resulting single mode energies are plotted in Fig. 3(b). In the presence of the anharmonic terms in the model, the instabilities that give the greatest lowering of energy are the Γ_{15}, R_{25}, and Σ_3 ones, exactly those instabilities which are primarily responsible for the Zr-rich PZT phase diagram.[45]

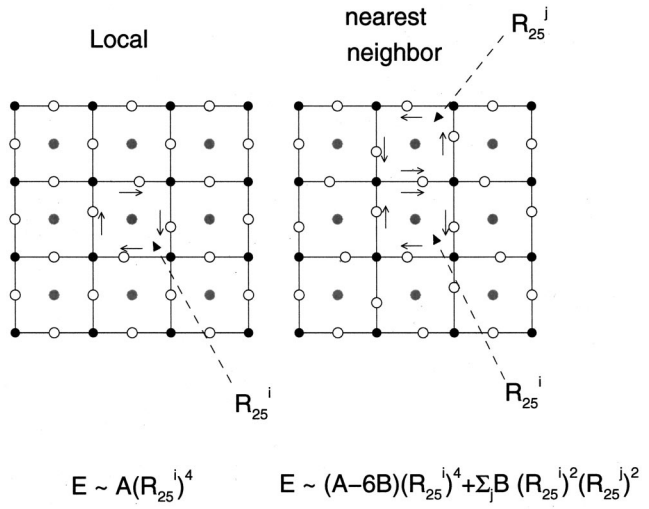

FIG. 5. Local and local plus nearest-neighbor quartic couplings for R_{25} oxygen octahedral tilts. By construction, both are consistent with the *ab initio* results depicted in Fig. 4.

C. R_{25} energy landscape

As alluded to above, nonlocal anharmonic couplings are introduced to the R_{25} displacement. The rationale is as follows. Suppose the *ab initio* potential-energy landscape (Fig. 4) is fitted to nonlocal harmonic terms obtained from *ab initio* linear-response calculations *and* local anharmonic terms (Fig. 5). In this case, the R_{25} oxygen octahedral tilts remain frozen in beyond $T \sim 1100$ K—which is above the temperature at which the ferroelectric order parameter vanishes. In other words, a spurious antiferrodistortive (AFD) phase is predicted, contrary to experiment.[1] This happens regardless of the functional form of the rest of H_{eff}.

A comparison with $SrTiO_3$ suggests why this might be expected. $SrTiO_3$ exhibits an antiferrodistortive phase which vanishes at $T=105$ K. *Ab initio* calculations indicate that the R_{25} potential energy well, obtained by freezing one Cartesian polarization component of the R_{25} mode, is of order 8 meV.[46] In PZT 95/5, the corresponding energy is ~ 40 times larger, and to a zeroth approximation the transition temperature should scale similarly. The two cases are not identical; in $SrTiO_3$, quantum effects are important, only one of the three Cartesian components of the R_{25} polarization is frozen in, and no ferroelectric modes are present. However, with the local anharmonic R_{25} interaction, the AFD structure in our PZT 95/5 model persists to temperatures at which the ferroelectric modes have disappeared; the comparison between the two cases is valid at these temperatures.

While we have not ruled out that the LDA is actually consistent with a spurious AFD phase in PZT 95/5, we find that the AFD behavior can be avoided by including nearest-neighbor anharmonic (quartic) couplings. (Fig. 5). This is because local and nearest-neighbor terms of opposite sign should favor localized oxygen octahedral tilting but destabilize correlated intercell oxygen octahedral tilting. In other words, the opposing terms reduce the correlation length and destroy long-range order. Furthermore, our nonlocal term does *not* contradict the *ab initio* potential-energy landscape; the small supercells used to map out the R_{25} energy landscape are fully consistent with nonlocal interactions of any range provided they fold to the same values (Fig. 5). Some forms of nonlocal anharmonic terms are also present in Ref. 29.

The magnitude of the local and nearest-neighbor quartic R_{25} interactions are described in the Appendix. Given that range is important, larger supercells can in principle be used to shed light on this issue. However, the multitude of possible terms needed to account for anisotropy makes this a daunting task. We believe a better way to assess the true range of the R_{25} anharmonic coupling would be to compare the phonon spectra of (say) the $F_{R(\mathrm{LT})}$ phase predicted both from first principles and from H_{eff}.[47]

D. M_3-Γ_{15} coupling

The M_3-Γ_{15} coupling also warrants further discussion. Experimentally, it is found that *M*-like superlattice reflections occur in the $F_{R(\mathrm{HT})}$ phase.[11–14] References 12–14 suggest the existence of M_3 modes, which in turn suggests that Γ_{15} and M_3 modes may cooperatively give rise to another low-energy structure which manifests itself at finite temperature.[48] We have investigated this possibility using an unstrained, doubled unit cell (lattice vectors [110], $[1\bar{1}0]$, and [001]) with a [111]-polarized Γ_{15} mode of fixed amplitude plus one of the three M_3 modes frozen in. We find that, regardless of the Γ_{15} and M_3 amplitudes, the energy of the unit cell is not lower than that of the simple $F_{R(\mathrm{HT})}$ structure, which has no M_3 distortions.

Next we allow all atoms in the doubled cell to relax after initially freezing in varying amplitudes of Γ_{15} and M_3. The results are not definitive because the system can be trapped in metastable states. To the best of our knowledge, having both types of distortions does reduce the energy from that of $F_{R(\mathrm{HT})}$ by ~ 5 meV per formula unit. The resulting structure, which, by symmetry, has no R_{25} distortions, is still much higher than the energy of $F_{R(\mathrm{LT})}$ (which does exhibit R_{25} octahedral tilts). This suggests that (a) only a small energetic advantage exists for having both *M*- and Γ-like distortions; and (b) the presence of M_3 distortions is secondary and incidental, and by itself does not significantly stabilize ferroelectric distortions to an extent that make the latter competitive with the A_{O} and $F_{R(\mathrm{LT})}$ structures. Reference 29 predicted a condensation of the Γ_{15} mode and three M_3 modes into a low-energy structure; our explicit LDA calculations show that this is likely an artifact of their parametrization. The simplified coupling scheme used in our H_{eff} neglects the small energetic advantage due to freezing in M_3 modes; hence the *M*-like superlattice reflections observed experimentally are not predicted by our model.

E. Fitting away from *ab initio* results

In several respects, we parametrized H_{eff} in ways which deviate from first-principles results, primarily to attain qualitative agreement with finite-temperature experiments. The effects of these changes will be commented upon again in later sections.

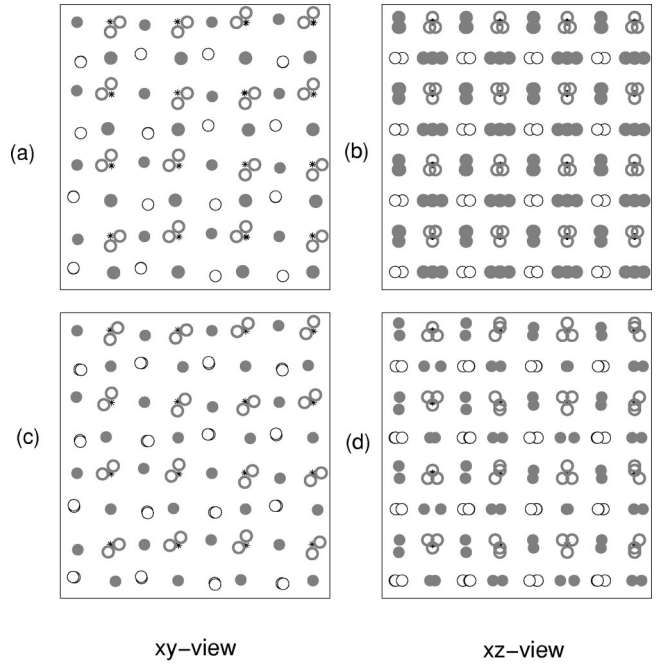

FIG. 6. Stable A_O structure for PZT 95/5 virtual crystal predicted by [(a) and (b)] an effective Hamiltonian and [(c) and (d)] the LDA. The empty and filled circles are for atoms on the Pb-site and Zr/Ti-site planes, respectively. The multiple projections of the atoms on the *xy* and *xz* planes show their positions in alternate crystal planes. See Sec. IV for details.

1. M_5'

The A_O phase exhibits Σ_3-like distortions. Using *ab initio* fitted parameters in H_{eff}, the energy obtained by freezing in Σ_3 with the LDA coupling parameter was 40% too low. We find that this leads to a disordering of the R_{25} oxygen tilts at low temperature in the A_O phase. (See Sec. V.) Therefore, we modified the coupling parameter by increasing the M_5' quartic term from its *ab initio* value by 40%. This reduces the overestimation of stabilization energy to 30%, as quoted in Sec. III B. We could not increase this parameter further because it raises the A_O energy without modifying the $F_{R(\text{LT})}$ energy, and it is necessary to keep the former as the stable phase.

2. Strain-phonon coupling

The volume of the A_O structure is too large in the uncorrected H_{eff}. A_O is dominanted by R_{25}- and Σ_3-like distortions. The Σ_3-strain coupling is not computed explicitly; its initial value in H_{eff} is related to the values of the Γ_{15} and $M_{5'}$ strain coupling parameters. To correct the A_O volume, we artificially increase the strain-$M_{5'}$ coupling.

3. Thermal expansion

Thermal expansion in a crystal depends on lattice anharmonicity and phonon-strain coupling. In the effective Hamiltonian approach used here, however, many such anharmonic and coupling terms are by necessity neglected; thermal expansion is therefore not expected to be accurately treated. However, it is a crucial factor in the PZT 95/5 antiferroelectric-ferroelectric phase transition, which exhibits a large volume change over a narrow range of temperature (see Ref. 1, Fig. 7.4). Therefore, we artificially inserted a negative pressure term $-\alpha_P T$, where $\alpha_P = 2.42$ meV K^{-1} or 5.56 MPa K^{-1}. If all strain-phonon coupling are ignored, this term gives a thermal expansion coefficient slightly (12%) larger than that of the experimental value for cubic PZ [$\alpha_{a'} = (-2.6\times10^{-5})\,^\circ\text{C}^{-1}$]. Thermal expansion has been computed in the literature from first principles for other materials.[49] In the case of PZT 95/5, the existence of three distinct phases and the large unit cells involved (up to 40 atoms) make this too expensive.

4. A_O-$F_{R(\text{LT})}$ energy difference

The energy of the $F_{R(\text{LT})}$ structure is raised by 9.0 meV per formula unit, so that it is now 12.3 meV above A_O. This is done by increasing the biquadratic anharmonic coupling terms between X_3-R_{25} and between M_5'-R_{25}. This increases the stability of the A_O phase at and near room temperature.

IV. STABLE STRUCTURE AT $T=0$ K

The harmonic part of H_{eff} was obtained from linear response calculations using $4\times4\times4$ **q** sampling. This is equivalent to calculations for a $4\times4\times4$ supercell. To extend the interatomic force matrix to larger cells, we follow the standard procedure of subtracting the long range dipole-dipole interaction from the interatomic force matrix in Fourier space, casting the remaining short-range part into a finite-ranged interaction, and adding the dipolar term back via the Ewald sum technique.[43,44] Dipolar interactions are long ranged and the simulation scales as $O(N^2)$, where N is the number of atoms in the system.

Due to the small energy difference between the A_O and $F_{R(\text{LT})}$ phases, simulated annealing (with the Metropolis updating scheme applied for up to 10 000 Monte Carlo passes) typically results in structures that contain signatures of both of these phases, as well as other new Fourier modes, but which are higher in energy than both. No simulated annealing runs have yielded energies lower than that of A_O. By slightly increasing the A_O-$F_{R(\text{LT})}$ energy difference to >15 meV (e.g., by increasing the R_{25}-M_5' isotropic, quartic repulsive term), the A_O structure is recovered reproducibly. By continuity, we assume this is the stable phase of H_{eff} even for A_O-$F_{R(\text{LT})}$ energy difference <15 meV. We have also considered a $6\times6\times6$ supercell, which is incommensurate with the Σ_3 mode. Again, the system tends to be trapped in metastable configurations. Using Fourier modes as degrees of freedom, we can project out all Γ-like ferroelectric distortions. The resulting structure resembles A_O in some respects but has a reproducible energy higher than that of the Σ-commensurate cells by ~0.02 eV per formula unit.

The stable A_O structure predicted by H_{eff} is compared to the LDA structure in Fig. 6 and Table III. We obtain qualitatively correct features. Σ_3 and R_{25} are the modes with largest frozen-in amplitudes, and R_{25} has a [110]-type polarization. We do not observe any frozen-in P_3 or X_3 modes. Because we do not truncate any degrees of freedom, it is

TABLE III. Amplitudes of most prominent lattice displacements for PZT 95/5 virtual crystal stable phase, predicted from the LDA and LDA-based effective Hamiltonian ground-state calculations. The effective Hamiltonian yields an energy of −0.3870 eV per formula unit for the metastable $F_{R(\mathrm{LT})}$ structure.

		LDA			Model		
q	Atom	*x*	*y*	*z*	*x*	*y*	*z*
1/4 1/4 0	Pb	0.0327	0.0327	0.0000	0.0387	0.0387	0.0000
(Σ)	O_1	0.0049	0.0336	0.0000	0.0040	0.0207	0.0000
	O_1'	0.0336	0.0049	0.0000	0.0207	0.0040	0.0000
	O_2	0.0314	0.0314	0.0000	0.0466	0.0466	0.0000
1/4 1/4 1/2	O_1	0.0000	0.0000	0.0154	0.0000	0.0000	0.0000
(*P*)	O_1'	0.0000	0.0000	0.0154	0.0000	0.0000	0.0000
	O_2	0.0096	0.0096	0.0000	0.0000	0.0000	0.0000
1/2 1/2 1/2	O_1	0.0000	0.0000	0.0705	0.0000	0.0000	0.0678
(*R*)	O_1'	0.0000	0.0000	0.0705	0.0000	0.0000	0.0678
	O_2	0.0689	0.0689	0.0000	0.0691	0.0691	0.0000
Energy (eV)			−0.3942			−0.3993	

possible to compare the atomic positions as well. The projections on the *xy* and *xz* planes are depicted in Fig. 6. The small Pb period doubling along the *z* axis seen in experiments[34] and in fully relaxed LDA predictions is due to P_3-like distortion and is not captured by H_{eff}. On the other hand, Fig. 6 shows that H_{eff} predicts oxygen positions projected onto the *xy* plane, which closely resemble LDA predictions. The agreement is less favorable in the *xz* plane, where some LDA-predicted superlattice structures are missing from the H_{eff} predictions. The $F_{R(\mathrm{LT})}$ metastable structure (not shown) closely resembles LDA predictions.

V. FINITE-TEMPERATURE BEHAVIOR

Finite-temperature simulations of the present H_{eff} are performed with $8\times8\times8$ supercells. $4\times4\times4$ cells give qualitatively and even quantitatively similar results.

The phases which can emerge from our simulations are sensitive to the form of H_{eff}. Among these possible phases, Σ_3-, R_{25}-, and Γ_{15}-like distortions either coexist or they compete. Furthermore, different polarizations of both the R_{25} and Γ_{15} distortions are possible. Let us first summarize the spurious phases that are obtained if we had not followed the changes listed in Sec. III C and E. (a) Using all *ab initio* parameters and local R_{25} local anharmonic terms, we obtain the sequence of phases $A_O\rightarrow\mathrm{AFD}\rightarrow P_C$ as temperature increases. (b) With the modifications of Sec. III E but not Sec. III C (i.e., with only local R_{25} anharmonic terms), an $F_{R(\mathrm{LT})}$ phase intervenes between A_O and AFD. (c) With all the modifications of Secs. III E and III C, we obtain the experimentally observed sequence $A_O\rightarrow F_{R(\mathrm{HT})}\rightarrow P_C$. In other words, AFD disappears and the $F_{R(\mathrm{LT})}$ is metastable to A_O in its entire range of stability; it transforms into $F_{R(\mathrm{HT})}$ at a low temperature, before either of the ferroelectric phases become thermodynamically more stable than A_O.

To arrive at the above conclusions, we have computed free-energy differences between the A_O and the ferroelectric phases. There is a substantial kinetic barrier for the $A_O\rightarrow F_{R(\mathrm{HT})}$ transition, which never spontaneously occurs for the $8\times8\times8$ supercell. Instead, in our calculations, we always start with either the A_O or $F_{R(\mathrm{LT})}$ phase, and slowly increase the temperature to study their properties. In particular, the transition temperature of the A_O to $F_{R(\mathrm{HT})}$ first-order phase transition is determined by comparing their Gibbs free energies:

$$-F(T)/T=\log \mathrm{Tr}\{\exp[-H_{\mathrm{eff}}(T)/T]\}. \tag{3}$$

Boltzmann's constant has been set to unity. The free energies are computed by thermodynamic integration, i.e., by tuning a reference Hamiltonian $H_{\mathrm{eff}}(\lambda=0)$ with analytically known free energies continuously onto the true effective Hamiltonian $H_{\mathrm{eff}}(\lambda=1)$:

$$-[F(1)-F(0)]=-\int_0^1 d\lambda\left\langle\frac{\partial H_{\mathrm{eff}}(\lambda)}{\partial\lambda}\right\rangle_\lambda .$$

The reference Hamiltonians used are Einstein crystals in which all atomic displacements experience a harmonic potential, with a force constant 2 a.u., centered at either the A_O or $F_{R(\mathrm{HT})}$ basis function positions. Along the thermodynamic integration paths, the temperature is fixed, and the simulation cells do not undergo *any* phase transitions. In other words, the two branches of the simulation with Hamiltonians $H_{\mathrm{eff}}(\lambda)$, remain in the A_O or $F_{R(\mathrm{HT})}$ phases for any value of λ within the temperature range of interest.

Without the artificial thermal expansion term of Sec. III E 3, no ferroelectric phase is observed at any temperature. With this term, the three experimentally observed phases are reproduced: (a) For $T<350$ K, A_O is stable. The Σ_3 mode and correspondingly polarized R_{25} mode are frozen in. The structure does not deviate strongly from the 0-K structure discussed above. The magnitudes of the most prominent frozen-in lattice distortions are depicted in Fig. 7(a). (b) For $350\ \mathrm{K}<T<898$ K, the $F_{R(\mathrm{HT})}$ phase results. Globally, the R_{25}-like oxygen tilts average to zero, i.e., at high temperature, a structure which is locally $F_{R(\mathrm{LT})}$-like averages macro-

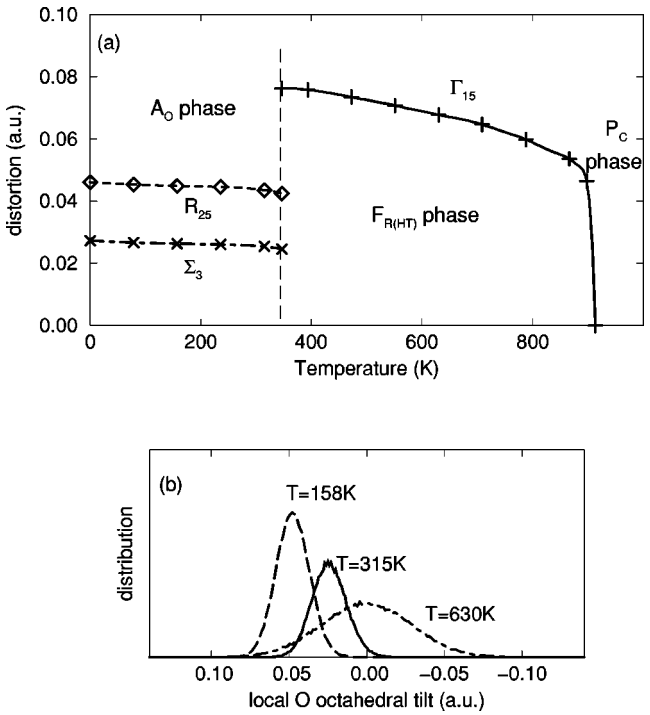

FIG. 7. (a) Mean amplitudes of various frozen-in modes, in units of a.u., as functions of temperature. Γ_{15} and R_{25} amplitudes are averaged over the three Cartesian directions. For convenience, Σ_3 only measures the size of the Pb displacement. The simulation is conducted using $8\times8\times8$ supercells starting with A_O and $F_{R(\mathrm{LT})}$ structures; the latter rapidly transform into the $F_{R(\mathrm{HT})}$ phase at temperature above $T\sim340$ K. The A_O-$F_{R(\mathrm{HT})}$ transition temperature is at $T=350$ K; this is determined from comparisons of their free energies (see the text). The $F_{R(\mathrm{HT})}$-P_{C} transition is at $T=898$ K. (b) The distribution of local oxygen octahedral tilt amplitudes, computed at temperatures below and above the oxygen tilt order-disorder transition temperature.

scopically to to the $F_{R(\mathrm{HT})}$ structure. Figure 7(b) illustrates the distribution of local R_{25}-like oxygen displacements in each primitive cell (modulated by the R-point wave vector). In the low-temperature $F_{R(\mathrm{LT})}$ (metastable) phase, the distribution of such local distortions indicates broken-symmetry. At high temperature (the $F_{R(\mathrm{HT})}$ phase), a single peak centered at zero tilt is observed, but the distribution is broad and its wings strongly overlap with the peak at low temperatures, indicating significant local distortions. These local distortions exist on a correlation lengthscale which is temperature dependent and spans roughly two primitive cells. As mentioned above, we do not observe M_3 oxygen tilts in the $F_{R(\mathrm{HT})}$ phase because it is not built into H_{eff}. From purely energetic considerations, M_3 modes only marginally enhance the stabilities of the rhombohedral ferroelectric phases. (c) The $F_{R(\mathrm{HT})}$ phase spontaneously transforms to the P_C phase at $T>898$ K. There is a large discontinuity in the Γ_{15} order parameter at this temperature, indicating a first-order transition.

The numerical uncertainty of our simulated A_O-$F_{R(\mathrm{HT})}$ transition temperature (T_{c1}) is about ±15 K. The experimental A_O-$F_{R(\mathrm{HT})}$ and $F_{R(\mathrm{HT})}$-P_C phase transitions occur at ~323 and 503 K, respectively.[1] Our corresponding transition temperatures are too high by 8% and 79%. These discrepancies are comparable to those of previous effective Hamiltonian predictions of transition temperatures.[25,26,28] Recall that T_{c1} is dependent on the lattice thermal expansion term as well as the energy difference (ΔE_1) between the A_O and $F_{R(\mathrm{LT})}$ structures. As discussed above, the ferroelectric phase vanishes if the thermal expansion term is not included. It also vanishes if ΔE_1 is increased substantially from the present value of 12.3 meV. The sensitivity of T_{c1} to ΔE_1 is about 7.5 K/meV. Given the uncertainty in ΔE_1, we have treated it as a fitting parameter to yield a phase transition temperature similar to that seen in experiments. We have not reduced it further because a spurious $F_{R(\mathrm{LT})}$ phase appears at ΔE_1 values which are too small. The $F_{R(\mathrm{HT})}$-P_C transition temperature (T_{c2}) does not strongly depend on the parameters of H_{eff}.

In the above, we neglected the effect of spatial inhomogeneities associated with Zr/Ti disorder.[10,51] Finally, our model gives $\Delta\alpha=0.233°$ at $T=315$ K, which is consistent with the trends of high Zr-content PZT at finite temperature.[10]

VI. CONCLUSIONS

We report three categories of results on PZT 95/5: first-principles predictions; 0-K structural predictions via an effective Hamiltonian H_{eff}, and finite temperature H_{eff} results. We presented LDA/VCA results for strain-relaxed structures of the A_O phase and (metastable) $F_{R(\mathrm{LT})}$ phases. These structures are very similar in energy. In contrast, the five-atom $F_{R(\mathrm{HT})}$ zero-temperature structure is much higher in energy and, more significantly, is unstable with respect to R_{25}-like oxygen octahedral tilts. This suggests that the antiferroelectric-ferroelectric phase transition in PZT 95/5 is governed to a large extent by the competition between the A_O and $F_{R(\mathrm{LT})}$ structures. We stress that this conclusion is drawn from *ab initio* results, not from effective Hamiltonian simulations.

Using first-principles linear-response/supercell calculations and a knowledge of the stable and metastable phase energies, we fitted an H_{eff} that yields A_O and $F_{R(\mathrm{LT})}$ phase atomic positions that are in reasonable agreement with LDA predictions. This is nontrivial because one of the main features of the A_O structure, the Σ_3-like distortions, is not directly fitted to LDA calculations of Σ_3 energetics. We note that, to our knowledge, this is the first successful modelling attempt to capture the fundamental features of the A_O phase in terms of condensation of unstable modes. As far as we know, no atomistic potential attempt has succeeded in this regard.

H_{eff} also describes PZT 95/5 behavior at finite temperature. It is found that, within the relatively simple form of H_{eff}, several departures from *ab initio* results have to be made. With these changes, we observe an antiferroelectric phase (A_O) below $T=350$ K, a paraelectric phase (P_C) above 898 K, and the $F_{R(\mathrm{HT})}$ phase in between. The predicted finite temperature $F_{R(\mathrm{HT})}$ contains spatially disordered oxygen octahedral tilts.

Apart from reproducing the experimentally observed sequence of phases for PZT 95/5,[1] and raising the critically

important issue of the closeness of the energies of the A_O and $F_{R(\mathrm{LT})}$ structures at zero temperature, we have also examined the possible role of M_3 tilt, which has been suggested in experiments[12–14] and theory[29] to coexist with the Γ_{15} distortions in the $F_{R(\mathrm{HT})}$ phase. Finally, we have investigated the energetics of R_{25} oxygen octahedral tilting, associated with the $F_{R(\mathrm{LT})}$-$F_{R(\mathrm{HT})}$ phase transition, and incorporated them into H_{eff}.

To conclude, we discuss this work in the context of effective Hamiltonian theory. For an effective Hamiltonian to be successful, two conditions must be met: (1) the Taylor expansion must accurately reproduce the low-energy landscape, and (2) anharmonic cross-terms involving neglected degrees of freedom must not have a significant effect on the thermodynamics of the system. We discuss how well our H_{eff} meets both of these conditions and compare our approach with previous effective Hamiltonian approaches.

Condition (1): The A_O LDA ground state of PZT 95/5 is very close in energy to a metastable $F_{R(\mathrm{LT})}$ phase. Because these two phases are so close in energy, explicitly enforcing the LDA energy ordering of the phases in an effective Hamiltonian seems highly desirable. Previous effective Hamiltonians have relied on a Taylor expansion out of a high-energy cubic structure to approximate the ground-state energy; in the present case, where two competing structures extremely close (a few meV) in energy exist, any attempt to reproduce the LDA energy ordering from a Taylor expansion alone is at best fortuitous and at worst impossible. This is the reason Ref. 29 fails to give the correct ground state, and by extension, a correct phase diagram.

In effective Hamiltonians for ferroelectric perovskites with a single Γ_{15} instability responsible for the observed phases transitions, an eighth-order Taylor expansion in powers of the instability vector components generally reproduces the low-energy landscape very accurately. In PZT 95/5 with several competing instabilities, comparable accuracy requires that both terms involving a single instability and cross-terms involving different instabilities be computed to eighth order. We did compute couplings to eighth order, but, due to the sheer number of coupling coefficients, we treated most couplings in an istotropic manner. Unlike the harmonic energy of the lattice, for which dispersion is calculated in creating an effective Hamiltonian; anharmonic first-principles calculations have generally been performed only for specific combinations of points in the Brillouin zone. The harmonic calculations thus have the necessary information for determining intersite coupling in the local variable representation used in simulations, but the anharmonic results do not. Thus, as previously done, we included only on-site anharmonic terms (or nearest-neighbor terms only for couplings between modes whose local representations are on different sites). Such a model however, does not give a reasonable $F_{R(\mathrm{LT})}$-$F_{R(\mathrm{HT})}$ transition temperature. We therefore introduced nearest-neighbor anharmonic quartic coupling in the R_{25} term in order to avoid a spurious antiferrodistortive phase in our simulation.

Condition (2): A full lattice Hamiltonian contains all anharmonic interactions not forbidden by symmetry, in particular couplings involving the *stable* modes. In the effective Hamiltonian approach, these terms are generally ignored (in effect, set to zero). To have a Hamiltonian in reduced degrees of freedom that precisely reproduces the thermodynamics of the full system, however, one must integrate the original partition function over the neglected degrees of freedom. One obtains an effective free energy in terms of the remaining degrees of freedom. This free energy has the form of an effective Hamiltonian with temperature-dependent coefficients. Most effective Hamiltonians for perovskite-type materials, however, attempt to reproduce the lattice dynamics with reduced degrees of freedom and *temperature-independent* coefficients. Indeed, this may be one of the major reasons why such effective Hamiltonians often give transition temperatures that are significantly different than experiment. When there are large transition temperature errors in a system with several competing phases, the resulting phase diagram can be completely wrong unless something is done to compensate for the effects of the neglected anharmonic terms.

One simple correction is to include a temperature-dependent thermal-expansion term directly into the Hamiltonian. Since thermal expansion in systems without lattice instabilities is generally linear, and since we already explicitly include the coupling of the instabilities with strain, it is reasonable to add a linear thermal expansion term to capture the effect of the coupling of the *stable* modes with strain. Indeed, in PZT 95/5, thermal expansion *not* directly involving the unstable modes must be included in order to obtain the correct phase diagram. Neglected anharmonic couplings will also affect the intramode and intermode coupling terms in our model, in some cases enough to give spurious phases in the phase diagram. Thus we adjusted coupling parameters between the appropriate modes. Although we adjusted these terms by adding a constant, the above discussion suggests that better agreement with the experimental phase diagram might be obtained by using temperature-dependent parameters. These considerations have proved crucial in reproducing the phase diagram of the very complex material PZT 95/5, but may be valuable in constructing effective Hamiltonian in other cases as well.

Our representation of independent instabilities by distinct local variables gives an obvious correspondence between the energetics of the instabilities and the interactions between the corresponding local variables. The couplings between different instabilities can easily be adjusted to see what effect(s) they have on the phase diagram. Given that competition between instabilities are ubiquitous in perovskite-type materials, our form of effective Hamiltonian is well-suited for this kind of investigation.

ACKNOWLEDGMENTS

We thank Peter Schultz, Umesh Waghmare, John Aidun, Tom Russo, Ellen Stechel, and Bruce Tuttle for their suggestions and useful input. K.L. and A.F.W. were supported by the Department of Energy under Contract No. DE-AC04-94AL85000. Sandia is a multiprogram laboratory operated by Sandia Corporation, a Lockheed Martin Company, for the U.S. Department of Energy.

TABLE IV. Coefficients of some anharmonic terms in the effective Hamiltonian. * indicates that the R_{25} isotropic quartic coupling is split into a local term (magnitude 365.85) and a nearest-neighbor term (magnitude -55; see Fig. 4). † indicates that the M_5' isotropic quartic term is increased from its *ab initio* value by 40%.

Mode	a_1	a_2	a_3	a_4	a_5	a_6	a_7	a_8	a_9
Γ_{15}	93.08	−796.1	4231	94.68	433.2	11.57	−5180	40682	1533
R_{25}	35.85*	−191.9	689.0	44.99	−128.9	544.3	2371	4563	183.6
M_5'	565.0†	−15312	407742	147.9	−51882	1854000	34136	NA	NA

APPENDIX: EFFECTIVE HAMILTONIAN PARAMETERS

For simplicity, all parameters are given in atomic units. We use an effective Hamiltonian H_{eff} of the form

$$H_{\text{eff}}=H_{\text{harmonic}}+H_{\text{anharmonic}}+H_{\text{strain}}(T)+H_{\text{strain coupling}}. \tag{A1}$$

H_{harmonic} governs the quadratic coupling of atomic displacements, including the long-ranged dipole-dipole coupling, and is given by

$$H_{\text{harmonic}}=(1/2)\sum_{ij\alpha\beta} x_{i\alpha}\Phi_{ij\alpha\beta}x_{j\beta}, \tag{A2}$$

where $x_{i\alpha}$ $(x_{i\alpha})$ are displacements of atom i (j) in the Cartesian direction α (β). $H_{\text{strain}}(T)$ is given by the VCA PZT 95/5 elastic constants $C_{11}=10.8851$, $C_{12}=2.9768$, and $C_{44}=8.0070$ per formula unit, along with an artificial temperature-dependent pressure. The form of $H_{\text{strain coupling}}$ was given in Ref. 29; the coupling parameters are $g_o=-3.0655$, $g_1=-7.6522$, and $g_2=-5.3309$ for Γ_{15}; and $g_o=7.4512$, $g_1=-6.6656$, $g_2=0$; M_5', $g_o=13.6335$, and $g_1=g_2=0$ for R_{25}. The R_{25} and M_5' strain couplings are first computed from finite differences, using the eigenvalues of the interatomic force matrix for different strained cells. Then, as mentioned in Sec. III E 2, the strain-M_5' coupling is artificially increased from first-principles results. The Γ_{15}-strain coupling terms are fitted to reproduce the lattice parameters and energetics of strain-relaxed, five-atom unit cells with rhombohedral, orthorhombic, and tetragonal symmetries. In principle, all phonon modes couple to strain. For convenience, we have only considered the R_{25}, M_5', and Γ_{15} modes, because their strain-coupling contributions appear to dominate the A_O and $F_{R(\text{LT})}$ structures.

$H_{\text{anharmonic}}$ is given by the expression

$$\begin{aligned}H_{\text{anharmonic}}=&H_1(\Gamma_{15})+H_1(R_{25})+H_{M_{5'}}+H_X+H_{\Gamma_{25}}\\&+H_3(\Gamma_{15},X_5)+H_3(\Gamma_{15},M_{5'})+H_3(\Gamma_{15},\Gamma_{25})\\&+H_3(R_{25},M_{5'})+H_3(R_{25},\Gamma_{15})+H_3(M_3,M_{5'})\\&+H_3(\Gamma_{15},M_3)+H_3(R_{25},M_3)\\&+H_{aniso}(\Gamma_{15},R_{25})+H_{intersite}(R_{25}).\end{aligned} \tag{A3}$$

The anharmonic terms involving the three polarization components of Γ_{15} and of R_{25} have the form:

$$\begin{aligned}H_1=\sum_s\ [&a_1(x_s^4+y_s^4+z_s^4)+a_2(x_s^6+y_s^6+z_s^6)+a_3(x_s^8+y_s^8\\&+z_s^8)+a_4(x_s^2y_s^2+x_s^2z_s^2+y_s^2z_s^2)+a_5[x_s^4(y_s^2+z_s^2)+y_s^4(x_s^2\\&+y_s^2)+z_s^4(x_s^2+y_s^2)]+a_6(x_s^4y_s^4+x_s^4z_s^4+y_s^4z_s^4)\\&+a_7(x_s^2y_s^2z_s^2)+a_8(x_s^4y_s^2z_s^2+y_s^4x_s^2z_s^2+z_s^4x_s^2y_s^2)\\&+a_9(x_s^6y_s^2z_s^2+y_s^6x_s^2z_s^2+z_s^6x_s^2y_s^2)],\end{aligned} \tag{A4}$$

where x_s, y_s, and z_s are the local projections of Γ_{15} and R_{25} types, centered on site s, described in the text. The coefficients $\{a_m\}$ are listed in Table IV.

There are six distinct $M_{5'}$ modes—two each for (1/2 1/2 0), (1/2 0 1/2), and (0 1/2 1/2). Their anharmonic energy is approximated as

$$\begin{aligned}H_{M_{5'}}=\sum_s\Bigg[&a_1\sum_{i=1,3,j=1,2}M_{ijs}^4+a_2\sum_{i=1,3,j=1,2}M_{ijs}^6\\&+a_3\sum_{i=1,3,j=1,2}M_{ijs}^8\Bigg]+\sum_{ss'}\Bigg[a_4\sum_{i<i'}\left(\sum_{j=1,2}M_{ijs}^2\right)\\&\times\left(\sum_{j'=1,2}M_{i'j's'}^2\right)\Bigg]+\sum_{ss's''}\Bigg[a_5\sum_{i<i'<i''}\left(\sum_{j=1,2}M_{ijs}^2\right)\\&\times\left(\sum_{j'=1,2}M_{i'j's'}^2\right)\left(\sum_{j''=1,2}M_{i''j''s''}^2\right)\\&+a_6\sum_{i<i'<i''}\left(\sum_{j=1,2}M_{ijs}^4\right)\left(\sum_{j'=1,2}M_{i'j's'}^2\right)\\&\times\left(\sum_{j''=1,2}M_{i''j''s''}^2\right)+a_7\sum_{i<i'<i''}\left(\sum_{j=1,2}M_{ijs}^6\right)\\&\times\left(\sum_{j'=1,2}M_{i'j's'}^2\right)\left(\sum_{j''=1,2}M_{i''j''s''}^2\right)\Bigg],\end{aligned} \tag{A5}$$

where i labels the wave vector, j its polarization direction, and s the site at which the basis functions are centered. Where more than one site is involved in Eq. (A5), they are constrained to be mutual nearest neighbors. The parameters are given in Table IV.

The anharmonicity of the six equivalent X_5 oxygen displacement modes is fitted to the form

$$H_X = \sum_s \left[b_1 \sum_{i=1,6} X_{is}^4 \right], \tag{A6}$$

with $b_1 = 6.195$. That of the three orientations of Γ_{25} is

$$H_{\Gamma_{25}} = \sum_s \left[\sum_{i=1,3} (d_1 \Gamma_{is}^4 + d_2 \Gamma_{is}^6 + d_3 \Gamma_{is}^8) \right], \tag{A7}$$

with $d_1 = 50.18$, $d_2 = -668.7$, and $d_3 = 4766.3$.

The cross-terms are all of the form

$$H_3(A,B) = (1/N_{\text{neigh}}) \sum_{ss'} \left[\sum_{ij} c_1 A_{is}^2 B_{js'}^2 + c_2 A_{is}^2 B_{js'}^4 + c_3 A_{is}^2 B_{js'}^6 \right], \tag{A8}$$

where i and j label the polarization components and/or (in the case of M-like modes) Brillouin, zone wave vector, and s and s' are constrained to be nearest neighbor pairs for the sublattices on which the two types of basis functions are centered. Since two functions pertaining to different modes can be centered on different atoms, the number of nearest neighbors (N_{neigh}) varies. In the following, the first mode listed is represented by "A_{is}" and the second by "$B_{js'}$." Γ_{15}-X_5: $c_1 = 98.0$, $c_2 = c_3 = 0$. Γ_{15}-M_5': $c_1 = 516.5$, $c_2 = -41317.9$, $c_3 = 1105927.8$. Γ_{15}-Γ_{25}: $c_1 = 41.59$, $c_2 = c_3 = 0$. R_{25}-M_5': $c_1 = 82.0$, $c_2 = c_3 = 0$. R_{25}-Γ_{15}: $c_1 = 52.5$, $c_2 = -1888.9$, $c_3 = 54868.5$. M_3-$M_{5'}$: $c_1 = 40.0$, $c_2 = c_3 = 0$. Γ_{15}-M_3: $c_1 = 20.0$, $c_2 = c_3 = 0$. R_{25}-M_3: $c_1 = c_2 = c_3 = 0$. Recall that the c_1's have all been adjusted to give A_O and $F_{R(\text{LT})}$ energies that are consistent with transition temperatures reported in this work. Note that there are no explicit anharmonic terms for M_3 modes. Their anharmonicity is governed by the R_{25} terms. We find, however, that it is necessary to use cross-couplings that involve M_3 to suppress certain spurious structures which compete with the A_O phase. Finally, the orientation-dependent interaction coefficient between Γ_{15} and R_{25} modes in Eq. (2) is $c^{(\text{aniso})} = 0.2$.

[1] B. Jaffe, W. J. Cook, and J. Jaffe, *Piezoelectric Ceramics* (Academic Press, London, 1971), pp. 139.

[2] I. J. Fritz and J. D. Keck, J. Phys. Chem. Solids **39**, 1163 (1978).

[3] Also see Z. Ujma, J. Handerek, and G. E. Kugel, Ferroelectrics **198**, 77 (1997), and references therein, concerning Nb doping in PZT 95/5.

[4] D. Berlincourt, H. Jaffe, H. H. A. Krueger, and B. Jaffe, Phys. Rev. Lett. **3**, 90 (1963); D. Berlincourt, H. H. A. Krueger, and B. Jaffe, J. Phys. Chem. Solids **25**, 659 (1964); D. H. Zeuch, S. T. Montgomery, and J. D. Keck, J. Geophys. Res., [Solid Earth] **98**, 1901 (1993); B. A. Tuttle, P. Yang, J. H. Gieske, J. A. Voigt, T. W. Scofield, D. H. Zeuch, and W. R. Olson, J. Am. Ceram. Soc. **84**, 1260 (2001).

[5] P. C. Lysne and C. M. Percival, J. Appl. Phys. **46**, 1519 (1975).

[6] H. M. Barnett, J. Appl. Phys. **33**, 1606 (1962).

[7] C. Michel, J.-M. Moreau, G. D. Achenbach, R. Gerson, and W. J. James, Solid State Commun. **7**, 865 (1969).

[8] R. Clarke and A. M. Glazer, Ferroelectrics **12**, 207 (1976).

[9] A. M. Glazer, S. A. Mabud, and R. Clarke, Acta. Crystallogr. Sect. B: Struct. Crystallogr. Cryst. Chem. **34**, 1060 (1978).

[10] D. L. Corker, A. M. Glazer, R. W. Whatmore, A. Stallard, and F. Fauth, J. Phys.: Condens. Matter **10**, 6251 (1998).

[11] J. Ricote, D. L. Corker, R. W. Whatmore, S. A. Impey, A. M. Glazer, J. Dec, and K. Roleder, J. Phys.: Condens. Matter **10**, 1767 (1998).

[12] D. Viehland, J.-F. Li, X.-H. Dai, and Z. Xu, J. Phys. Chem. Solids **57**, 1545 (1996).

[13] X.-H. Dai, Z.-K. Xu, and D. Viehland, J. Am. Ceram. Soc. **78**, 2815 (1995).

[14] D. Viehland, J.-F. Li, X.-H. Dai, and Z. Xu, Ferroelectrics **183**, 311 (1996).

[15] B. Noheda, J. A. Gonzalo, and M. Hagen, J. Phys.: Condens. Matter **11**, 3959 (1999).

[16] J. Ricote, R. W. Whatmore, and D. J. Barber, J. Phys.: Condens. Matter **12**, 323 (2000).

[17] N. Cereceda, B. Noheda, T. Iglesias, J. R. Fernandez-del-Castillo, J. A. Gonzalo, N. Duan, Y.-L. Wang, D. E. Cox, and G. Shirane, Phys. Rev. B **55**, 6174 (1997).

[18] Somewhat similar issues are addressed for PZT 50/50 supercells in Ref. 19.

[19] M. Fornari and D. J. Singh, Phys. Rev. B **63**, 092101 (2001).

[20] D. J. Singh, Ferroelectrics **194**, 299 (1997); Phys. Rev. B **52**, 12 559 (1995).

[21] N. J. Ramer and A. M. Rappe, Phys. Rev. B **62**, 743 (2000); J. Phys. Chem. Solids **61**, 315 (2000).

[22] L. Bellaiche and D. Vanderbilt, Phys. Rev. Lett. **83**, 1347 (1999).

[23] Ph. Ghosez, E. Cockayne, U. V. Waghmare, and K. M. Rabe, Phys. Rev. B **60**, 836 (1999).

[24] E. Cockayne and K. M. Rabe, J. Phys. Chem. Solids **61**, 305 (2000).

[25] A non-exhaustive list of *ab initio* effective Hamiltonian studies include K. M. Rabe and J. D. Joannopoulos, Phys. Rev. Lett. **59**, 570 (1987); Phys. Rev. B **36**, 6631 (1987); K. M. Rabe and U. V. Waghmare, Ferroelectrics **164**, 15 (1995); **194**, 119 (1996); W. Zhong, D. Vanderbilt, and K. M. Rabe, Phys. Rev. Lett. **73**, 1861 (1994); Phys. Rev. B **52**, 6301 (1995); L. Bellaiche, A. Garcia, and D. Vanderbilt, Phys. Rev. Lett. **84**, 5427 (2000).

[26] U. V. Waghmare and K. M. Rabe, Phys. Rev. B **55**, 6161 (1997).

[27] H. Krakauer, R. Yu, C.-Z. Wang, K. M. Rabe, and U. V. Waghmare, J. Phys.: Condens. Matter **11**, 3779 (1999).

[28] L. Bellaiche, A. Garcia, and D. Vanderbilt, Phys. Rev. Lett. **84**, 5427 (2000).

[29] U. V. Waghmare and K. M. Rabe, Ferroelectrics **194**, 135 (1997); U. V. Waghmare, Ph.D. thesis, Yale University, 1996.

[30] See L. Bellaiche and D. Vanderbilt, Phys. Rev. B **61**, 7877 (2000), and references therein, for a discussion of virtual crystal approximation applied to perovskites.

[31] The nomenclature of the phonon modes follow R. A. Cowley, Phys. Rev. **134A**, 981 (1964).

[32] K. Leung and A. F. Wright (unpublished).

[33] H. Fujishita and S. Hoshino, J. Phys. Soc. Jpn. **53**, 226 (1984); H. Fujishita, Y. Shiozaki, N. Achiwa, and E. Sawaguchi, *ibid.* **51**, 3583 (1982), and references therein.

[34] H. Fujishita, S. Katano, J. Phys. Soc. Jpn. **66**, 3484 (1997): H. Fujishita and S. Katano, Ferroelectrics **217**, 17 (1998).
[35] K. M. Rabe and U. V. Waghmare, Phys. Rev. B **52**, 13 236 (1995).
[36] G. B. Bachelet, D. R. Hamann, and M. Schluter, Phys. Rev. B **26**, 4199 (1982).
[37] N. Troullier and J. L. Martins, Phys. Rev. B **43**, 1993 (1991).
[38] A. M. Rappe, K. M. Rabe, E. Kaxiras, and J. D. Joannopoulos, Phys. Rev. B **41**, 1227 (1990).
[39] S. G. Louie, S. Froyen, and M. L. Cohen, Phys. Rev. B **26**, 1738 (1982).
[40] H. J. Monkhorst and J. D. Pack, Phys. Rev. B **13**, 5188 (1976).
[41] Phenomenological models fit to experimental data have assumed both first- and second-order phase transitions for the disordering of the oxygen tilts. See M. J. Haun, E. Furman, T. R. Halemane, and L. E. Cross, Ferroelectrics **99**, 55 (1989) and references therein, and Ref. 17.
[42] As discussed in Ref. 32, the relaxation of both strain and cation positions in LDA calculation of the A_O phase is crucial to making the latter more stable than $F_{R(\mathrm{LT})}$.
[43] P. Giannozzi, S. de Gironcoli, P. Pavone, and S. Baroni, Phys. Rev. B **43**, 7231 (1991).
[44] X. Gonze, J.-C. Charlier, D. C. Allan, and M. P. Teter, Phys. Rev. B **50**, 13 035 (1994).
[45] Note that, in this mode-by-mode analysis, we have made no effort to ensure particular basis sets for the degenerate eigen modes, and instead used whatever modes resulted from diagonalizing the IFM. For example, the three R_{25} modes obtained do not have polarizations parallel to the crystal axes. To harmonic order, the total energy is invariant with respect to the polarization direction. This is no longer true in presence of anharmonic terms, and these three modes, when relaxed one by one, give slightly different energies. Hence Fig. 3 is intended as a qualitative guide only.
[46] W. Zhong and D. Vanderbilt, Phys. Rev. Lett. **74**, 2587 (1995); N. Sai and D. Vanderbilt, Phys. Rev. B **62**, 13 942 (2000).
[47] These issues will be examined again in K. Leung (unpublished).
[48] Note, however, that Ref. 11 ascribes these *M*-like superlattice reflections to cation motions, not oxygen tilts.
[49] Representative *ab initio* calculations of bulk thermal expansion include S. Biernacki and M. Scheffler, Phys. Rev. Lett. **63**, 290 (1989); S.-Q. Wei, C.-L. Li, and M. Y. Chou, Phys. Rev. B **50**, 14 587 (1994); A. A. Quong and A. Y. Liu, *ibid.* **56**, 7767 (1997).
[50] M. A. Rodriguez (unpublished).
[51] S. Kojima, N. Ohta, and X.-L. Dong, Jpn. J. Appl. Phys. **38**, 5674 (1999).